



Open Archive Toulouse Archive Ouverte (OATAO)

OATAO is an open access repository that collects the work of Toulouse researchers and makes it freely available over the web where possible.

This is an author-deposited version published in: <http://oatao.univ-toulouse.fr/>
Eprints ID: 9317

To cite this document: Lv, Peng and Prothin, Sebastien and Mohd Zawawi, Fazila and Benard, Emmanuel and Morlier, Joseph and Moschetta, Jean-Marc *Study of A Flexible Blade for Optimized Proprotor*. (2013) In: ERCOFTAC International symposium Unsteady separation in fluid-structure interaction, 17-21 Jun 2013, Mykonos, Greece.

Any correspondence concerning this service should be sent to the repository administrator: staff-oatao@inp-toulouse.fr

STUDY OF A FLEXIBLE BLADE FOR OPTIMIZED PROPROPOTOR

Peng LV, Sebastien PROTHIN, Fazila MOHD-ZAWAWI,
Emmanuel BENARD, Joseph MORLIER,
Jean-Marc MOSCHETTA

*Université de Toulouse; Institut Clément Ader; ISAE, UPS, EMAC, INSA;
10 av. Edouard Belin, F-31055 Toulouse, France*

Abstract.

In the present study, a passive twist control is considered as a potential way to improve the overall flight efficiency for proprotor of Micro Air Vehicle (MAV). This paper will focus on the aerodynamic performance and deformation behaviour of a flexible laminate blade. Incorporated with a database of airfoil characteristics, Blade Element Momentum Theory (BEMT) is implemented for performance prediction of proprotor at low Reynolds numbers. The preliminary procedure is based on finding optimum twist distributions for hover and forward flight, but keeping a given chord distribution. A numerical model is developed using a combination of aerodynamic model based on BEMT, and structural model based on anisotropic beam finite element, in order to evaluate the coupled structural and the aerodynamic characteristics of the deformable proprotor blade. The numerical model - Fluid Structure Interaction (FSI) was then validated by means of shape reconstruction from LDS (Laser Displacement Sensor) outputs. It can be concluded that the proposed experiment technique is capable of providing a predictive and reliable data in blade geometry and performance for rotor mode. The FSI approach is also valid as a reliable tool for designing and analyzing the MAV proprotor made of composite material.

Key words: tilt-body MAVs, flexible proprotor, composite laminate, FSI, LDS.

1 Introduction

Tilt-rotor aircraft has been developed be multifunctional in order to offer a wide range of services. It can fly in both of hover and forward flight. In early 1950s, tilt-rotor aircraft was started to be developing. XV-3 of Bell company operated first transition from hover to forward flight. In 1970s, XV-15 was developed by Bell company to demonstrate the feasibility of tilt-rotor concept. Then it was moved to NASA and the U.S. Army for further study in aeroelasticity. The successful XV-15 led to the project of V-22. V-22 is the world's first production tilt-rotor aircraft. With respect to a proprotor of tilt-rotor aircraft, in hover, the inflow velocity is small and the proprotor must provide high thrust to support aircraft weight. By contrast, in forward flight, the inflow velocity is relatively large and the low thrust is just to overcome the drag. The difference in the inflow and thrust requirement between the two flight modes suggests different blade twist and chord distributions. In 1983, McVeigh obtained the twist of XV-15 proprotor through linear interpolation

of twist between rotor and propeller by a compromise [1]. Although this trade-off provided acceptable performance on XV-15, the stiff proprotor with certain twist cannot maximize the efficiency for both flights. In 1988, Nixon proposed a passive blade twist control method for the proprotor of XV-15 [2]. The study demonstrated successfully the feasibility of the passive blade control on conventional tilt-rotor aircraft. The tilt concept of typical aircraft attracts interest of researchers who are working on MAVs. In 2008, Shkarayev and Moschetta introduced the efforts on the aerodynamic design of a tilt-body MAV named miniVertigo, which had a tilt-body configuration [3]. The wind tunnel measurements were conducted for a motor, a wing, and an arrangement of a wing with a motor. The results were realized in the design of a prototype of tilt-body MAV which was successfully tested in flight. The small proprotors also suffer the problem caused by different twist between hover and forward flight. However, due to the small size of MAV, the complex tailored blade cross section for passive twist control based on conventional tiltrotor aircraft is not available any more on it. Therefore, composite laminate is explored to be a more practical method for proprotor blade of MAVion, which is a tilt-body MAV developed by ISAE. In this study, a passive twist control is considered as a potential way to improve the overall flight efficiency of MAV proprotor. The proprotor blade made of composite material is preferred to be used. It is due to their potential benefits such as aeroelastic tailoring, ability to manufacture, more refined aerodynamic designs, significant enhancements in fatigue performance and damage tolerance of the blade. The blade is expected to be deformed in torsion under different airloads and structural loads. This paper is aimed at developing an evaluation of design techniques of a composite flexible proprotor.

The key issue to study flexible blade is to observe the deformation accurately. Optical measurement techniques have been developing for a couple of years in applications of aerodynamics, materials and structure, such as Holographic Interferometry (HI), Electronic Speckle Pattern Interferometry (ESPI), Projection Moiré Interferometry (PMI) and Digital Image Correlation (DIC) [4]. In 1998, Fleming obtained the 3-D deformation of rotor blade using PMI technique [5]. However, it has low sensitivity for in-plane deformation and moderate for out-of-plane deformation. By contrast, DIC has a relatively high sensitivity that can reach 1/30,000 of the test field [6]. In 2011, Lawson demonstrated the deformation of a rotating blade using DIC [7]. The technique was found to have many advantages including high resolution results, non-intrusive measurement, and good accuracy over a range of scales. However, DIC needs a preprocessing which is to apply a stochastic speckle pattern to the surface by spraying it with a high-contrast and non-reflective paint. This complex painting will probably affect the stiffness of blade. Hence, in this study, LDS was developed to measure blade deformation and validate the FSI model.

2 Aerodynamic modelling

The aerodynamic model based on BEMT is used as a tool to compute the aerodynamic loadings. In the classical approach of rotor analysis, lift polar is a linear function [8]. Hence, in order to consider non-linear airfoil characteristics prevalent in low Reynolds number regime (generally, $Re < 70,000$), a database of airfoil char-

acteristics was incorporated into modified BEMT. To solve the BEMT equations, the blade should be numerically discretized into a series of small elements. In the classical equation,

$$4F\lambda^2 r dr = \frac{\sigma C_{l\alpha}}{2} (\theta r^2 - \lambda r) dr, \quad (1)$$

where λ is inflow ratio, F is Prandtl's tip-loss factor, r is nondimensional radius, dr is the nondimensional length of each element, $C_{l\alpha}$ is 2-D lift-curve-slope of airfoil, and θ is the pitch angle at the midspan of each element. By contrast, in the modified version, the incremental thrust coefficients are described using lift coefficient C_l directly instead of lift-slope $C_{l\alpha}$,

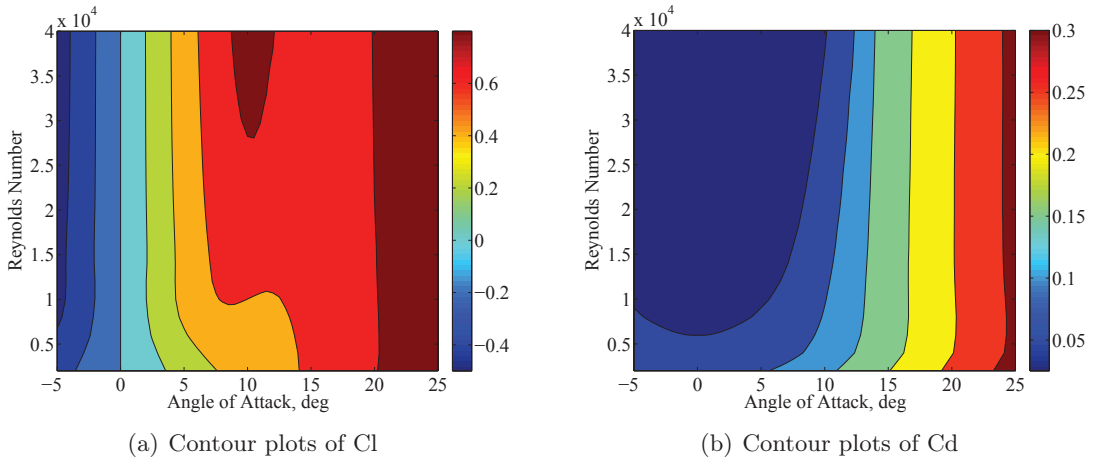


Figure 1: Airfoil characteristics of NACA0012

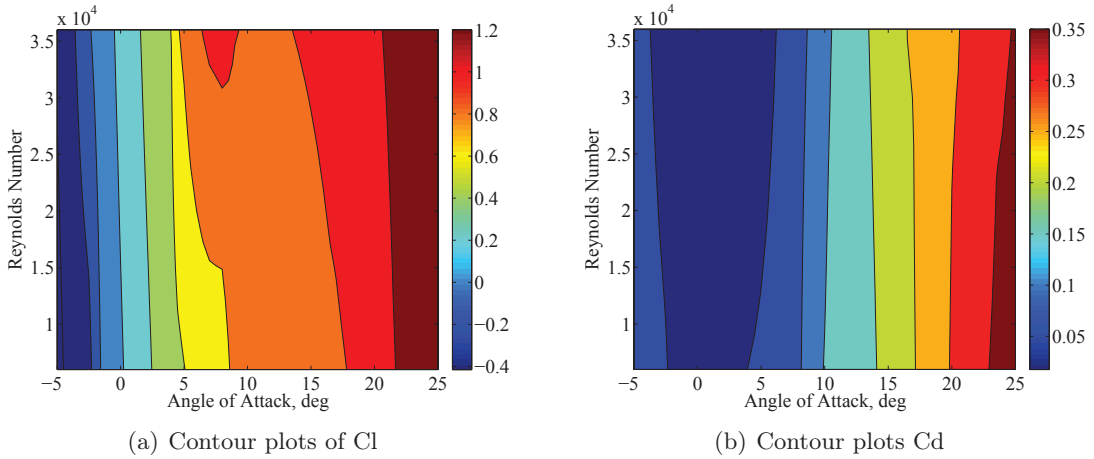


Figure 2: Airfoil characteristics of modified MA409

$$4F\lambda^2 r dr = \frac{1}{2} \sigma C_l r^2 dr. \quad (2)$$

Eq. 2 allows for the solution of induced flow ratio along the blade radius for a given rotor with certain chord distribution, collective pitch, twist distribution and airfoil

section. The result will be converged through a few iterations. In propeller analysis, the form of BEMT developed by Adkins was employed [9]. In this model, the inflow ratio or inflow angle is iteratively computed until the convergence criteria are reached. The database of airfoil characteristics are obtained from Xfoil, which is an airfoil design and analysis code developed by Drela [10]. BEMT model was validated using existing performance data of rotor and propeller. The detailed geometries of them are described in [11] and [12]. The airfoil of rotor defined by NACA0012 while the propeller airfoil is based on a modified MA409. Xfoil can not always give a converged solution of airfoil performance for given airfoils. Hence, in order to obtain a smooth database for BEMT convergence, it is necessary to conduct interpolation for lift coefficient C_l , drag coefficient and C_d and moment coefficient C_m with variation to angle of attack and Reynolds numbers. The N_{crit} to predict the flow transition is 0.1 for rotor and 7.0 for propeller corresponding to different turbulence intensities [12, 13]. Fig. 1 and Fig. 2 show the interpolated results on C_l and C_d . Fig. 3 and Fig. 4 exhibit the validation of performance predictions of the rotor and propeller. The BEMT model over predicts the thrust of rotor slightly while the torque matches well with experiment data. This is probably from that, as the wake becomes turbulent for heavy loading, air with momentum is transported from the outer flow region into the wake. The accuracy of BEMT model is decreased by the strong self-induction wake. Also, under heavy disk loading, the assumption of rigid wake sheet for Prandtl tip-loss function becomes not accurate enough. With respect to propeller, it is found that the developed BEMT method incorporated with database agrees better with the experimental data compared to the linear model Qprop [14]. However, for high disk loadings, the results predicted by Qprop which is capable of considering self-induction wake, show potentially better trends.

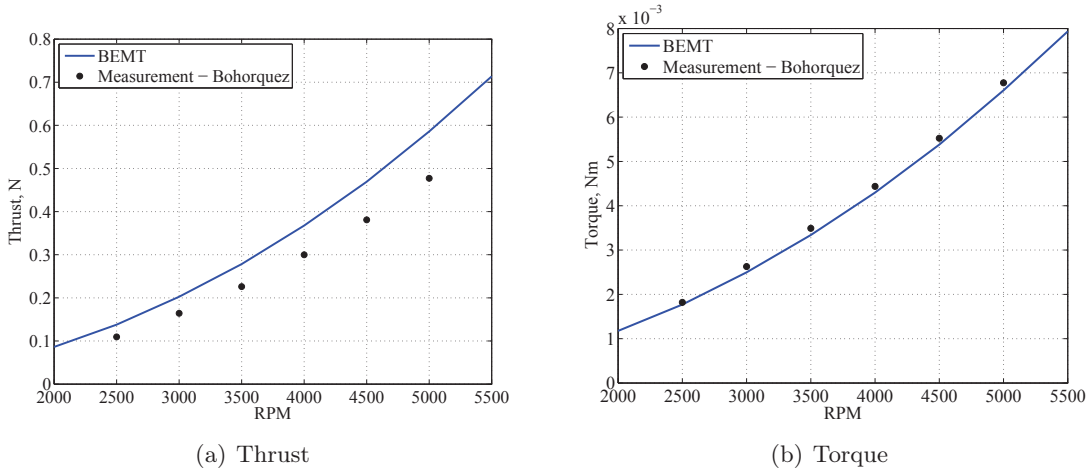


Figure 3: BEMT validation for rotor

Overall, the BEMT is an efficient tool for at least preliminary analysis of the spanwise distribution of airloads, especially due to the negligible computational cost of this method.

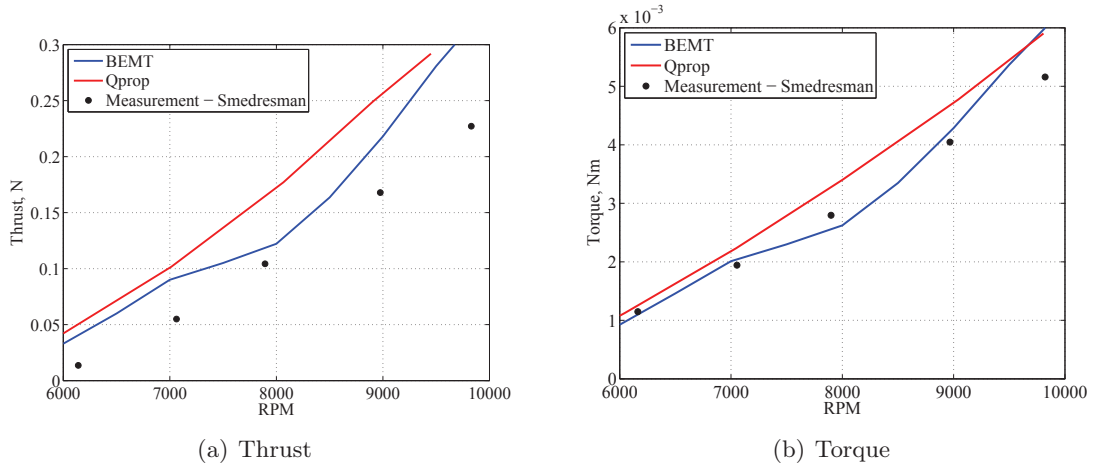


Figure 4: BEMT validation for propeller

Number of blades	Radius (m)	Hub radius (m)	Chord (m)	Built-in twist (deg)
2	0.2	0.03	0.03	-10/-15/-20/-25/-30

Table 1: The blades with varied built-in twist

	Hover	Forward flight
RPM	1500	1200
Velocity (m/s)	0	10
Advance ratio, J	/	1.25
Thrust (N)	2	0.3
Thrust coefficient	0.01	0.003

Table 2: Operation conditions of MAVion

3 Twist effect on the efficiency of small proprotor

In order to study the twist effect on the efficiency of small proprotor, five blades with varied built-in twist are defined first, as shown in Tab. 1. For example, twist -10 represents that twist of blade tip is lower than the counterpart of blade root by 10° with linear distribution. The airfoil of the blade is flat plate with a thickness of 2.5%. Tab. 2 exhibits the operation conditions for both hover and forward flight. Fig. 5(a) shows the twist effect on hovering efficiency - Figure of Merit (FM) with the variation to thrust coefficient. Thrust coefficient is adjusted by collective pitch for the five blades. The blade with built-in twist 10° has the maximum efficiency at $C_T=0.01$. In Fig. 5(b), the propulsive efficiencies of the five blades are all analyzed under $C_T=0.003$. They vary with the advance ratios in forward flight. The blade with twist 30° exhibits highest efficiency of all at advance ratio $J=1.25$. Overall, as we can see from Fig. 5, high twist of blade is beneficial for forward flight while low twist can improve hovering efficiency. According to the mission requirement of MAVion, the solution of proprotor for MAVion is given in Tab. 3.

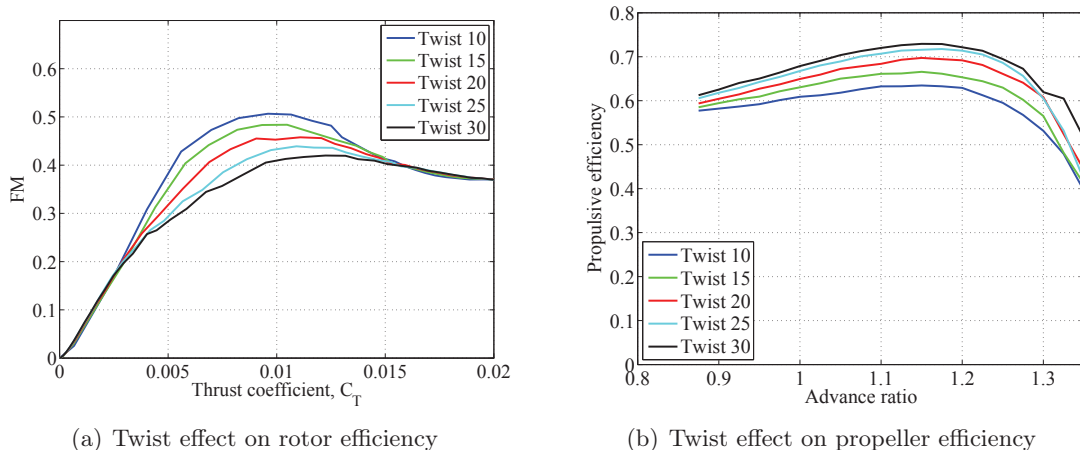


Figure 5: Twist effect to small proprotor

	Hover	Forward flight
Built-in twist (degree)	10	30
Collective pitch (degree)	31	54

Table 3: Optimized proprotor of MAVion

4 FSI Model

In order to compute the blade deformation under airloads and centrifugal loads, the coupled FSI model of the proprotor combines the aerodynamic model - BEMT and structural analysis model - FBEAM, which was developed by Mohd-Zawawi [15]. To begin with, the basic geometry (zero deflections) is assumed. Then the structural model calculates the blade deformations under airloads and centrifugal loads. The deformed blade shape is used to update the aerodynamic model. The quasi-steady aerodynamic loads are computed for the update geometry, using the 2D aerodynamic theory based on BEMT. The aerodynamic loads are transferred to the beam nodes as concentrated forces. A new structural analysis is performed to calculate the deformed shape of the blade under the influence of aerodynamic and centrifugal loads. The variation of the blade twist angle along the blade is monitored for convergence. The interaction is repeated until equilibrium between deformation and loadings is achieved. After convergence the proprotor performance characteristics are computed. The approach described above was applied to the constant chord untwisted 2-bladed system for small proprotor made of laminate composite. The deflection results in two basic modes of deformation; spanwise bending and torsion. The effects of camber changes are not included in this study due to limitation in the modeling. Firstly, a static analysis on a rectangular planform with dimension (length 190.5mm, width 12.7mm, thickness 3.175mm) was performed. Carbon/Epoxy with material properties $E_{11}=129\text{GPa}$, $E_{22}=9.4\text{GPa}$, $E_{33}=9.4\text{GPa}$, $G_{12}=5.16\text{GPa}$, $G_{13}=4.3\text{GPa}$, $G_{23}=2.54\text{GPa}$, $\mu=0.3$ and $\rho=1550\text{kg/m}^3$ was used. The ply angle with respect to pitch axis was 30° . The result obtained in FBEAM was validated by commercial structural analysis program namely MSc. Nastran and the validation result is illustrated in Fig. 6.

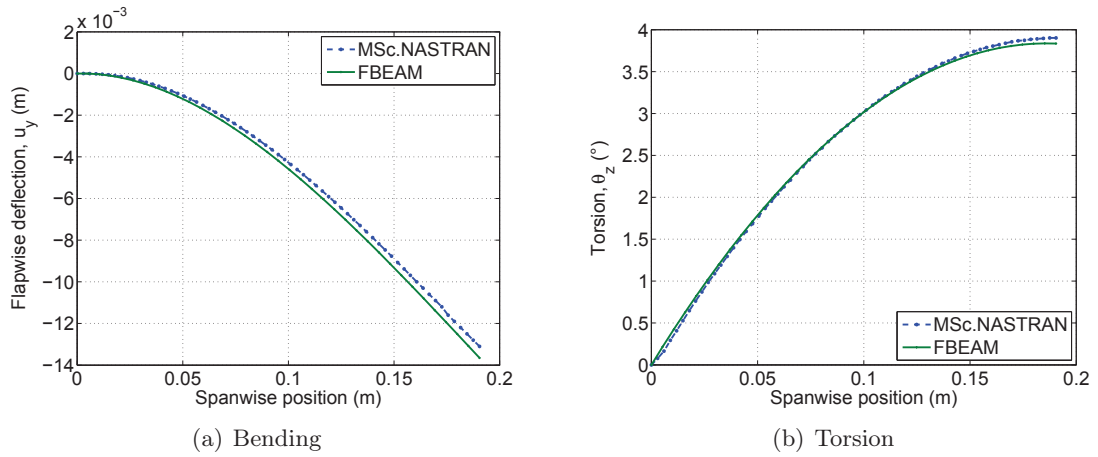


Figure 6: Static validation of FBEAM

5 Experimental setup

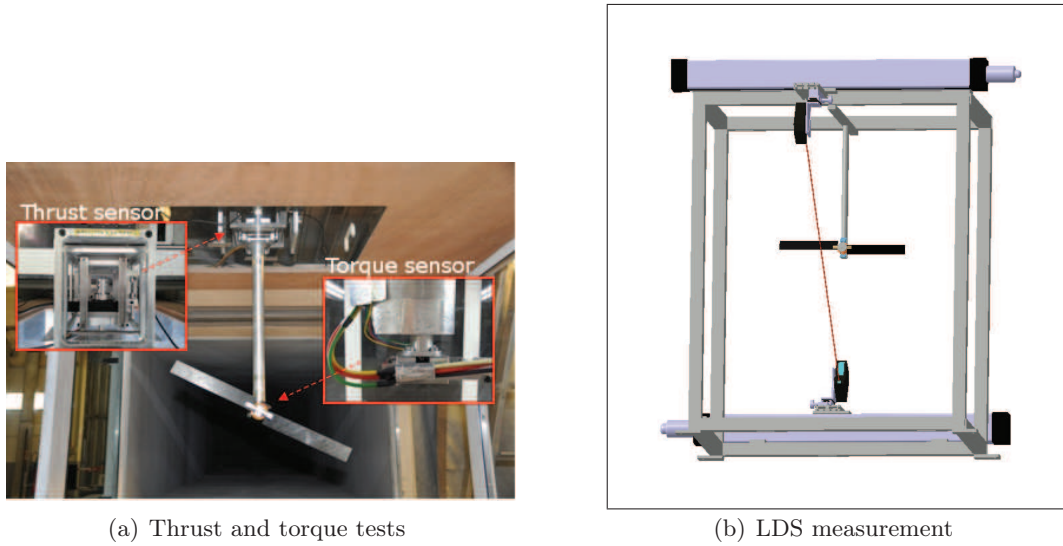


Figure 7: Experimental rigs

The blade was fabricated using Carbon/Epoxy with a stacking sequence $[45]_5$, and clamped with a collective pitch 15° . The geometry properties are the same with counterparts in Tab. 1 but without built-in twist. The two blades were driven by a high torque brushless motor - ATI 2208/24. To evaluate the flexible blade performance, the thrust and torque were measured using two transducers. The close-up view of the sensors and mounted blade can be seen in Fig. 7(a). In order to reconstruct the rotating blade, two LDSs are driven by track systems to scan the blade from blade root to tip with an incremental distance 2mm (Fig. 7(b)). The LDS used in experiment is KEYENCE LK-G502. The distance of reference is 500mm, and the range of measuring can be between -250mm to 500mm. The sampling frequency of this laser was selected as 10,000Hz. LDS records the Z coordinates (along the direction of height) which is the distance from the position detected on blade surface

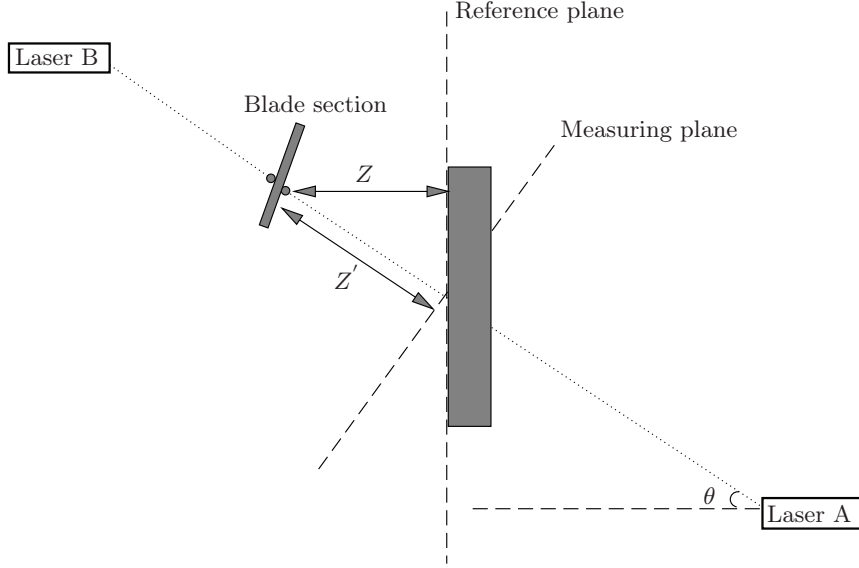


Figure 8: Measuring principle

to reference plane. Meanwhile, square wave in time domain is measured by optical RPM sensor. Then, average RPM and angular speed at each blade section can be extracted from the square wave. Furthermore, with the azimuth of feathering, polar coordinates is possible to be transferred to Cartesian coordinates X (along spanwise of blade) and Y (along chordwise of blade). Combining coordinates X , Y and Z , a polynomial surface fitting is performed to obtain the bending and torsion of rotating blade. As we can see, coordinates Z can be measured in a direct way by laser. However, coordinates X and Y are instead calculated by local radius of each scanning, angular speed of blade and sampling time,

$$X = r \cos(\omega t) = r \cos\left(\frac{\text{RPM}}{60} 2\pi t\right), \quad (3)$$

$$Y = r \sin(\omega t) = r \sin\left(\frac{\text{RPM}}{60} 2\pi t\right), \quad (4)$$

where r , ω and t are local radius, angular speed and sampling time, respectively. The uncertainties U_X and U_Y are defined by bias limits and precision limits using the Root-Sum-Square (RSS) method [16],

$$U_X = (B_X^2 + P_X^2)^{\frac{1}{2}}, \quad (5)$$

$$U_Y = (B_Y^2 + P_Y^2)^{\frac{1}{2}}, \quad (6)$$

where B_X , P_X , B_Y and P_Y are bias limits of X , precision limits of X , bias limits of Y and precision limits of Y . They are defined by,

$$\left(\frac{B_X}{X}\right)^2 = \left(\frac{1}{X} \frac{\partial X}{\partial r} B_r\right)^2 + \left(\frac{1}{X} \frac{\partial X}{\partial \text{RPM}} B_{\text{RPM}}\right)^2 + \left(\frac{1}{X} \frac{\partial X}{\partial t} B_t\right)^2, \quad (7)$$

$$\left(\frac{P_X}{X}\right)^2 = \left(\frac{1}{X} \frac{\partial X}{\partial r} P_r\right)^2 + \left(\frac{1}{X} \frac{\partial X}{\partial \text{RPM}} P_{\text{RPM}}\right)^2 + \left(\frac{1}{X} \frac{\partial X}{\partial t} P_t\right)^2, \quad (8)$$

$$\left(\frac{B_Y}{Y}\right)^2 = \left(\frac{1}{Y} \frac{\partial Y}{\partial r} B_r\right)^2 + \left(\frac{1}{Y} \frac{\partial Y}{\partial \text{RPM}} B_{\text{RPM}}\right)^2 + \left(\frac{1}{Y} \frac{\partial Y}{\partial t} B_t\right)^2, \quad (9)$$

$$\left(\frac{P_Y}{Y}\right)^2 = \left(\frac{1}{Y} \frac{\partial Y}{\partial r} P_r\right)^2 + \left(\frac{1}{Y} \frac{\partial Y}{\partial \text{RPM}} P_{\text{RPM}}\right)^2 + \left(\frac{1}{Y} \frac{\partial Y}{\partial t} P_t\right)^2, \quad (10)$$

With respect to the real Z of blade to reference plane, as shown in Fig. 8, it is defined by,

$$Z = Z' \cos(\theta), \quad (11)$$

where coordinates Z' are the distance data to measuring plane obtained from LDS directly, θ is the measuring angle of lasers. This is to say, coordinates Z are needed to be transformed from measuring system to the reference system for the reconstruction of blade shape. U_Z , it is defined by uncertainty of laser measurement directly,

$$U_Z = (B_{laser}^2 + P_{laser}^2)^{\frac{1}{2}}, \quad (12)$$

where B_{laser} and P_{laser} are bias limits and precision limits of laser data. All of bias limits are constants and they will not be affected by sampling. Local radius r is totally determined by track system while time t is from quartz crystal reference. Here, the precision limits of RPM are considered for uncertainties of coordinates X and Y . The precision limit of RPM is defined as,

$$P_{\text{RPM}} = \frac{1.96\sigma_{\text{RPM}}}{\sqrt{N_{\text{RPM}}}}, \quad (13)$$

where σ_{RPM} is the standard deviation of RPM and N is the RPM sampling number. The distance to a reference was measured by laser sensor first to study precision limits of coordinates Z , the precision of displacement data is defined as,

$$P_{laser} = \frac{1.96\sigma_{laser}}{\sqrt{N_{laser}}}, \quad (14)$$

where σ_{laser} is the standard deviation of measured distance by laser and N is the laser sampling number.

6 Results

The laminate blade was tested at RPM 1,500 in hover mode. The comparison results between BEMT model and experiments in performance are shown in Fig. 9. The errorbars represent the stand deviation of the mean of sampling data. In simulation, the input blade geometry for BEMT was assumed without deformation. As can be seen, the BEMT agrees well with experimental data of torque. However, it over-predicts the thrust. This is probably caused by the obvious bending deformation of rotating blade since it can generate the thrust vector in spanwise of blade. The precision limits of reference measurement was given by -35.8452 ± 0.0008 , as shown in Fig. 10(a). Besides, according to user's manual of KEYENCE LK-G502, when the detection range is between -250mm and 500mm , the bias limits is given by $\pm 0.1\%$. Based on Eq. 11, the uncertainty of coordinates Z is $\pm 0.1\%$. This is to say, compared with bias limits, precision limits of laser can be negligible. The normal density of RPM samples from optic sensor are shown in Fig. 10(b). Finally, the uncertainty of RPM was given by $1,517.5 \pm 11.4$. The uncertainty U_X and U_Y were calculated using

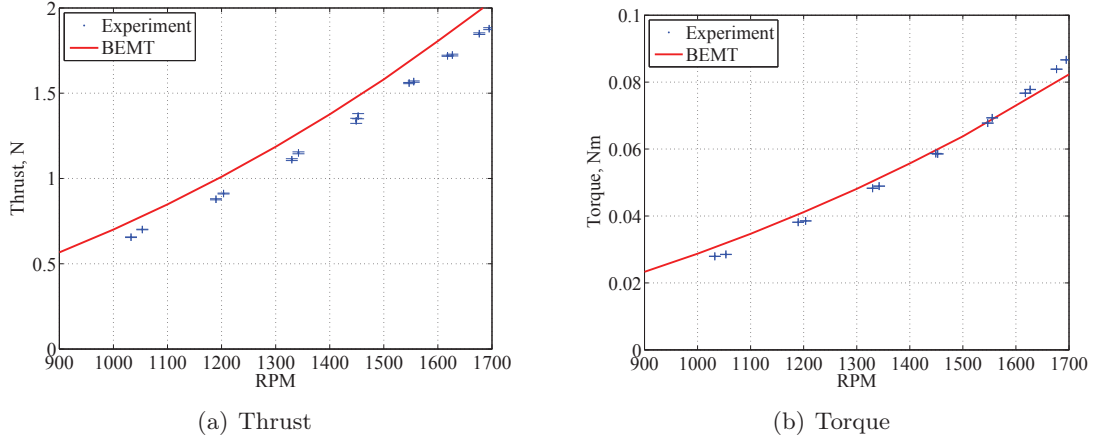


Figure 9: Aerodynamic performance of laminate blade

Eq. 5 and 6, as shown in Fig. 11 and 11. The blade was reconstructed through 3-D polynomial surface fitting of second order (Fig. 13(a)). Fig. 13(b) shows the bending distribution of rotating blade, and the errorbars are defined by the standard deviation of surface fittings along spanwise of blade. FSI simulation and experiment are capable of obtaining the bending distribution with approximately same order of magnitude. However, the curvatures of bending in FSI model and measurement are different especially around the blade root. The difference could be from composite properties in FSI model. Hence, it is necessary to measure the properties instead of using ideal characteristics. Also, initial scanning position of LDS may cause the curvature difference in bending.

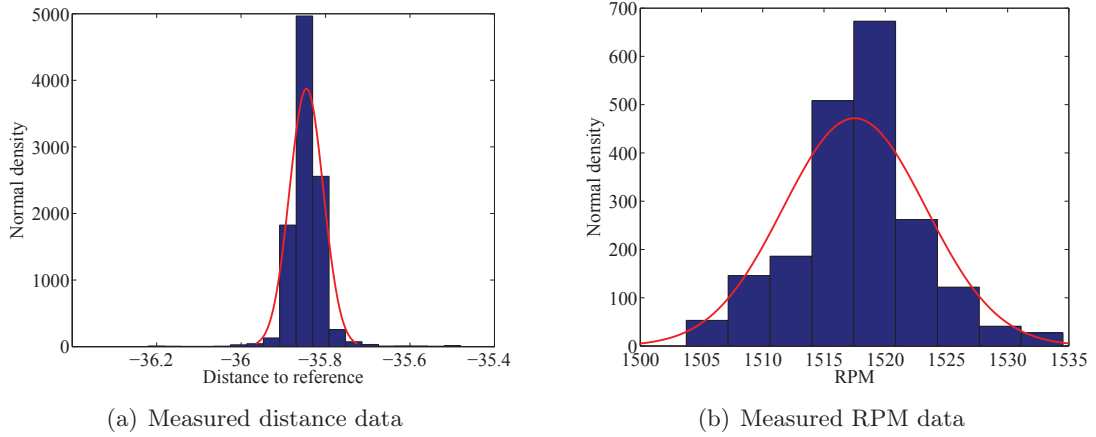


Figure 10: Normal density distribution

7 Conclusion

In conclusion, the evaluation of design techniques, both for the aerodynamic performance and for the structural behavior of a composite flexible proprotor has been presented in rotor mode. The numerical model BEMT has capability of prediction in proprotor aerodynamics. The results show high twist of blade is suitable for

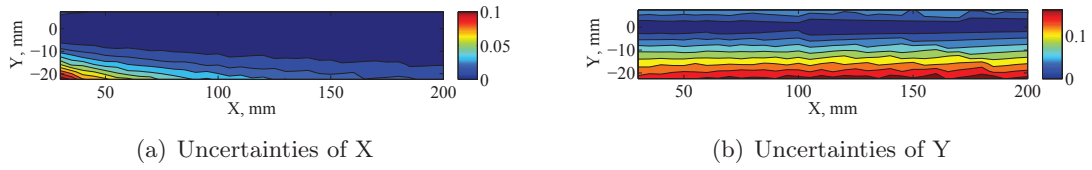


Figure 11: Uncertainties on upper surface

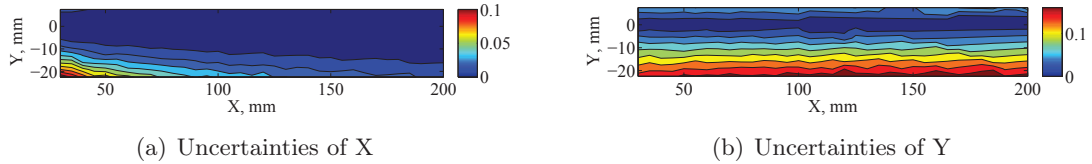


Figure 12: Uncertainties on lower surface

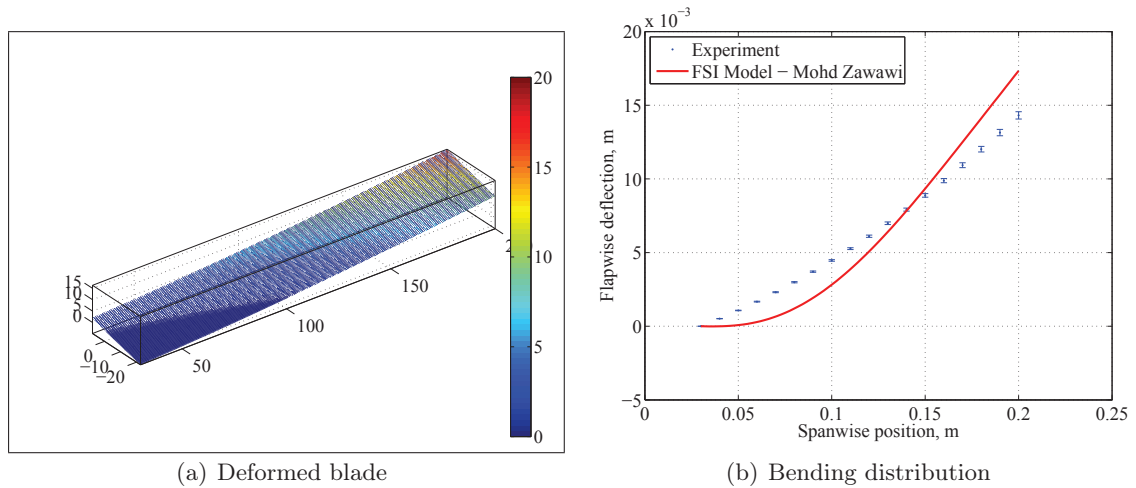


Figure 13: LDS results

propulsive efficiency while low twist is beneficial for hovering efficiency. FSI model has also been validated by LDS technique. The difference of bending distribution is expected to be studied further in terms of materials properties and experiment procedure. It can be concluded that the developed numerical model is a reliable tool for designing and analyzing the proprotor made of composite material. Additionally, current laminate was not observed deforming in beneficial torsion. In future, in order to obtain obvious torsion, the study will focus on the configuration design of laminate blade. Likewise, the experiments will also be expanded to propeller mode.

Acknowledgements

The authors thank Rémy CHANTON, Patrick MOREL, Philippe BARRICAU, Serge GERARD, Patrick CAZENAVE, Philippe MOULIGNE and Xavier FOULQUIER for advice and assistance. The research is supported by China Scholarship Council (CSC) and Malaysian government.

References

- [1] McVeigh M.A., Rosenstein H.J. 1983 Aerodynamic design of the XV-15 advanced composite tilt rotor blade *39th Annual Forum of the American Helicopter Society* 72-80
- [2] Nixon M.W. 1988 Improvements to tilt-rotor performance through passive blade twist control. *NASA Technical Memorandum 100583* 1-9
- [3] Shkarayev S., Moschetta J.M., Bataille B. 2008 Aerodynamic design of micro air vehicles for vertical flight. *Journal of Aircraft* **45** 1715-1724
- [4] Williams D. C. 1993 Optical methods in engineering metrology. *Chapman and Hall*
- [5] Fleming G. A., Gorton S. 1998 Measurement of rotorcraft blade deformation using projection moire interferometry. *Proceedings of the Third International Conference on Vibration Measurements by Laser Techniques: Advances and Applications, SPIE—the International Society for Optical Engineering, Ancona, Italy* 514-527
- [6] Schmidt T., Tyson J., Galanulis K. 2003 Full-field dynamic displacement and strain measurement using advanced 3D image correlation photogrammetry: Part 1. *Experimental Techniques* **27** 47-50
- [7] Lawson M.S., Sirohi J. 2011 Measurement of deformation of rotating blades using digital image correlation. *52nd AIAA/ASME/ASCE/AHS/ASC Structures, Structural Dynamics and Materials Conference, Denver, Colorado* **AIAA 2011-1876** 1-15
- [8] Leishman, J.G. 2006 Principles of helicopter aerodynamics. *Cambridge Aerospace Series, 2nd edition*
- [9] Adkins C.N. 1990 Design of optimum propellers. *Journal of Propulsion and Power* **10** 676-682
- [10] Drela M. 1989 An analysis and design system for low Reynolds number airfoil, low Reynolds number aerodynamic. *Springer-Verlag, New York* 1-12
- [11] Bohorquez F. 2007 Rotor hover performance and system design of an efficient coaxial rotary wing micro air vehicle. *Ph.D thesis, University of Maryland*
- [12] Smedresman A., Yeo D., Shyy W. 2011 Design, fabrication, analysis, and testing of a micro air vehicle propeller. *29th AIAA Applied Aerodynamics Conference, Honolulu, Hawaii* **AIAA 2011-3817** 1-16
- [13] Schafroth D.M. 2010 Aerodynamics, modeling and control of an autonomous micro helicopter. *Ph.D thesis, ETHZ*
- [14] Drela M. 2007 Qprop user guide. *MIT*
- [15] Moha-Zawawi F., Prothin S., Lv P., Benard E., Moschetta J.M., Morlier J. 2013 Study of a flexible UAV proprotor *48th International Symposium of Applied Aerodynamics Saint-Louis*. **FP30-2013** 1-10
- [16] Taylor J. R. 1996 An introduction to error analysis: the study of uncertainties in physical measurements. *University Science Books, Sausalito, California*